



Contents lists available at ScienceDirect

European Journal of Medicinal Chemistry

journal homepage: <http://www.elsevier.com/locate/ejmech>

Research paper

Design and synthesis of emodin derivatives as novel inhibitors of ATP-citrate lyase

Steffi K. Koerner^a, Jun-ichi Hanai^{b,c}, Sha Bai^a, Finith E. Jernigan^a, Miwa Oki^b, Chieko Komaba^b, Emi Shuto^b, Vikas P. Sukhatme^{b,c,d,**}, Lijun Sun^{a,*}^a Center for Drug Discovery and Translational Research, Department of Surgery, Beth Israel Deaconess Medical Center, Harvard Medical School, Boston, MA 02215, USA^b Divisions of Interdisciplinary Medicine and Biotechnology, Department of Medicine, Beth Israel Deaconess Medical Center, Harvard Medical School, Boston, MA 02215, USA^c Nephrology and Department of Medicine, Beth Israel Deaconess Medical Center, Harvard Medical School, Boston, MA 02215, USA^d Hematology-Oncology, Department of Medicine, Beth Israel Deaconess Medical Center, Harvard Medical School, Boston, MA 02215, USA

ARTICLE INFO

Article history:

Received 6 October 2016

Received in revised form

6 December 2016

Accepted 8 December 2016

Available online 9 December 2016

Keywords:

Emodin anthraquinones and anthracenone

ATP citrate lyase inhibitor

Lipogenesis

Cancer stem cell

ABSTRACT

Aberrant cellular metabolism drives cancer proliferation and metastasis. ATP citrate lyase (ACL) plays a critical role in generating cytosolic acetyl CoA, a key building block for *de novo* fatty acid and cholesterol biosynthesis. ACL is overexpressed in cancer cells, and siRNA knockdown of ACL limits cancer cell proliferation and reduces cancer stemness. We characterized a new class of ACL inhibitors bearing the key structural feature of the natural product emodin. Structure-activity relationship (SAR) study led to the identification of **1d** as a potent lead that demonstrated dose-dependent inhibition of proliferation and cancer stemness of the A549 lung cancer cell line. Computational modeling indicates this class of inhibitors occupies an allosteric binding site and blocks the entrance of the substrate citrate to its binding site.

© 2016 Elsevier Masson SAS. All rights reserved.

1. Introduction

Metabolic changes are a common feature of cancerous tissues. Mutations in oncogenes and tumor suppressor genes cause alterations to multiple intracellular signaling pathways that rewire tumor cell metabolism and re-engineer it to allow enhanced survival and growth. The extensive metabolic rewiring of malignant cells offers a large number of potential drug targets [1]. A proper intervention in a cancer metabolic pathway might provide a therapeutic advantage that can help overcome resistance to chemotherapy or radiotherapy [2].

The best characterized metabolic phenotype observed in tumor cells is the Warburg effect, which is a shift of ATP generation from

oxidative phosphorylation to glycolysis, even under normal oxygen concentrations [3]. This effect is regulated by PI3K, hypoxia-inducible factor (HIF), p53, MYC and AMP-activated protein kinase (AMPK)–liver kinase B1 (LKB1) pathways. Another metabolic pathway often increased in cancer cells is lipid synthesis. Adenosine triphosphate (ATP) citrate lyase (ACL) is the cytosolic enzyme that catalyzes the synthesis of acetyl-CoA from citrate. Cytosolic acetyl-CoA is the requisite building block for endogenous synthesis of fatty acids, cholesterol and isoprenoids, as well as for post-translational modification of proteins via acetylation. ACL is upstream of the other lipogenic enzymes and connects glucose metabolism (a way of generating acetyl CoA) and lipogenesis [4]. ACL also affects mitochondrial homeostasis and membrane potential through the increased availability of mitochondrial citrate for full oxidation and NADH production in the TCA cycle [5].

In tumor cells, *de novo* fatty acid synthesis occurs at high rates [6–8]. ACL was identified as a highly expressed protein in many tumors, including the chemoresistant colorectal cancer cells via unbiased proteomic profiling [9]. In agreement with reported results [4,10], our own data demonstrated that ACL knockdown (KD) by shRNA limits tumor cell proliferation and survival, induces

* Corresponding author. Center for Drug Discovery and Translational Research, Department of Surgery, Beth Israel Deaconess Medical Center, Harvard Medical School, Boston, MA 02215, USA.

** Corresponding author. Divisions of Interdisciplinary Medicine and Biotechnology, Department of Medicine, Beth Israel Deaconess Medical Center, Harvard Medical School, Boston, MA 02215, USA.

E-mail addresses: vsukhatm@bidmc.harvard.edu (V.P. Sukhatme), lsun1@bidmc.harvard.edu (L. Sun).

differentiation *in vitro* and *in vivo*, and reduces tumor growth in a number of animal models [11]. We have recently shown that ACL KD also targets cancer stem-like cells (CSCs) in multiple cancer types, suggesting that ACL inhibitors might be effective in reducing cancer stemness [12]. The presence of CSCs is believed to be a major underlying reason for the emergence of resistance to standard therapy and the occurrence of metastasis, major causes of treatment failure and mortality. Collectively, available data strongly support the notion that targeting ACL by small molecule inhibitors is an attractive strategy for developing an innovative cancer therapy to address the highly unmet needs in metastasis and drug resistance of cancers [13–16].

Nature is a rich source for biologically active compounds, including the widely used anticancer therapeutics paclitaxel and doxorubicin. The natural product 2-chloro-1,3,8-trihydroxy-6-methyl-10H-anthracen-9-one (**2a**), which is structurally related to emodin (**1a**) isolated from the Chinese herbal plant *Rheum palmatum* L. [17], was reported to display inhibitory activity against the ACL enzyme [18]. Herein we describe the structure-activity relationship (SAR) study of emodin anthraquinones and anthracenone, the characterization of potent ACL inhibitors, and their *in vitro* anticancer activities. Further, we show for the first time that small molecule ACL inhibitors reduce cancer stemness in breast and lung cancer 3D spheroid assays.

2. Results and discussion

2.1. Chemistry

The commercially available natural product emodin (**1a**) provides a unique template for the synthesis of structurally diverse derivatives. Our synthetic efforts were first directed at the synthesis of halogenated emodins (Fig. 1, Table 1). Mono-chlorinated emodin **1b** and **1c** are naturally occurring compounds that were extracted from lichen species and also obtained by biosynthesis utilizing isolated lichen enzymes [19]. Their regioselective syntheses however remains unexplored. Chen and Huang described that treatment of emodin **1a** with acetic acid and hydrochloric acid followed by H₂O₂ yielded the product **1c** together with two dichloroemodin derivatives in an equalmolar ratio [20]. A nonselective multistep synthesis of **1b** has been reported by both Yosioka et al. [19] and Sargent et al. [21]. We were able for the first time to regioselectively synthesize **1b** and **1c** in excellent yield. By applying the procedure developed by Elban and Hecht [22], we prepared **1b** in up to 85% isolated yield through treatment of **1a** with N-chlorosuccinimide (NCS) and zirconium chloride. The method was also applicable to the regioselective synthesis of compound **4** from the trimethylated emodin [23]. Conversely, the regioisomeric **1c** was formed exclusively and isolated in 80% yield by treating **1a** with sulfonyl chloride. ¹H NMR spectra supported the structural assignment, which was also found to be in agreement with literature values [24]. Regioselective iodination or bromination of **1a** produced the 3-iodoemodin **1e** and the 3,5-bisbromoemodin (**1d**), respectively, by following literature reported methods [25]. Subsequently, **1d** and **1e** underwent Suzuki coupling reactions [26] with a variety of aryl or heteroaryl boronic reagents to produce a series of aryl substituted derivatives (**1f–o**). Finally, using reported literature procedures [27], we prepared a series of Mannich reaction products (**1p–s** and **3a–b**) from emodin (**1a**), which were not explored further due to their extremely low solubility.

While substantial effort was devoted to the synthesis of the anthracenone natural product **2a**, we were not able to fully characterize the product, which we believe was primarily due to its instability as indicated in the literature [18]. Thus, when **1b** was subjected to tin (II) chloride mediated reduction condition - a

reliable method to regioselectively reduce the 10-carbonyl group of emodin [28], the reduction resulted exclusively in the dechlorinated product **2b**. When emodin anthracenone (**2b**) was treated with sulfonyl chloride, the novel 5-chlorinated anthracenone (**2c**) was isolated as a pale yellow powder (Fig. 1). The chemical structure of **2c**, in particular the position of the Cl substituent, was confirmed unequivocally by ¹³C-HSQC and ¹³C-HMBC NMR spectra indicating chlorination at the 4-position. But disappointingly, the treatment of **2b** with NCS and zirconium chloride failed to yield the expected 2-chlorinated anthracenone (**2a**). Instead, a dark complex mixture was formed under a variety of conditions. Attempts to manipulate the reactions by protecting the free hydroxyl groups, including the known tri-methylated derivative **4** (Fig. 1), all failed to generate the desired product **2a**. In our hands, **2b** and **2c** were stable as dry solids. In DMSO, however, they were only stable when kept at -20 °C and in the dark, and decomposed to a brown mixture after standing overnight at room temperature. It is known that the natural product emodin anthrone **2a** undergoes free radical mediated oligomerization to form polyaromatics [29,30]. We hypothesize the presence of an electron-withdrawing Cl group in **2c** (as well as in **2a**) increases the production of free radicals and decreases the stability of the compounds.

2.2. ACL enzymatic activity

Historically, the *in vitro* enzymatic activity of ACL, as well as its inhibition by inhibitors, was measured by the maleate dehydrogenase catalyzed reduction of oxaloacetate by NADH [31,32]. The method lacks high sensitivity, is laborious and inadequate for high-throughput screening. We instead applied the ADP Glo assay to measure directly the concentration of the enzymatic reaction product ADP and obtained high assay stability (CV value < 10%, S/B ratio > 25, Z'-factor > 0.7). Under our assay conditions, the IC₅₀ of the known ACL inhibitor BMS-303141 ranged from 0.3 to 0.5 μM, which is within the range of reported values of 0.94 μM by a ¹⁴C radioisotope assay and 0.13 μM by the traditional maleate dehydrogenase catalyzed reduction assay [33,34].

Table 1 summarizes the inhibitory activity of the newly synthesized emodin derivatives. Representative dose-response curves of ACL inhibition by lead compounds are shown in Fig. 2. As noted, at highest concentrations tested, the inhibitors were able to completely abolish the ACL enzymatic activity.

In agreement with previous literature, emodin (**1a**) and emodin anthrone (**2b**) are completely inactive at concentrations as high as 10 μM.ref.¹⁸ The halogenated emodin derivatives **1b–e** are among the more potent inhibitors in our series. The two mono-chlorinated emodins **1b** and **1c** are similarly active, with an IC₅₀ of 12.6 and 9.6 μM, respectively. The iodo derivative **1e** (IC₅₀: 7.5 μM) is slightly more active than its chloro counterpart (**1b**). With an IC₅₀ of 2.9 μM, the bisbromo derivative **1d** is the most potent in this series. Compound **2c**, the regioisomer of the reported natural product emodin anthracenone **2a**, potently inhibits ACL activity (IC₅₀: 3.8 μM), a 2.5-fold increase in potency from its anthraquinone analog **1c**.

The 2-aryl and 2-heteroaryl derivatives (**1f–o**) proved to be moderately active at best, with the pyrazole compound **1o** (IC₅₀: 13.3 μM) being the most active in this series. While the phenyl group in **1f** does not render it an active inhibitor, the addition of a methoxy (**1i**, **1j**) at the 3- or 4-position, or a methyl (**1g**) at the 3-position but not at the 4-position (**1h**), of the phenyl group result in moderately active inhibitors. In addition, the mono- and bis- 3-pyridyl derivatives (**1l**, **1n**) are also moderately active, while the 4-pyridyl isomer (**1m**) is not. The Mannich reaction products **1p–r** are inactive but their conformationally restrained tetracyclic analogs **3a–b** are moderately active, which may suggest that the 2-

position of emodin occupies a tight hydrophobic pocket on the ACL protein, that favors rigid substituents over bulky and flexible alkyl groups. Furthermore, it is worth noting that the moderate activity by **3a–b** indicates, that the 3-OH group of emodin is not absolutely required for the inhibition of ACL although it likely contributes to the overall potencies. On the other hand, one or perhaps both of the two OH groups surrounding the carbonyl group is critical for activity as the tri-methylated analog **4** is completely inactive (0% inhibition at 10 μM).

2.3. Docking studies

Sun et al. recently reported the co-crystal structure of a truncated ACL in complex with citrate, which revealed a network of H-bonds between the substrate and hydrophilic residues including Arg-379, Asn-346 and Thr-348 [35]. The natural product anthracenone **2a** has been previously described as a citrate competitive ACL inhibitor [18]. To investigate potential key interactions between **2a** and ACL protein, we performed auto docking studies to analyze low energy binding poses of **2a** in the ACL crystal structure (PDB: 3MWD). The top scoring binding pose (calculated binding energy: $E = -8.6$ kcal/mol) was identified and found to occupy an allosteric hydrophobic cleft directly adjacent to the substrate binding domain of ACL protein (Fig. 3a). The identified low energy binding pose of **2a** may have blocked the entrance of citrate to the binding site (indicated by a red arrow), which we theorize is responsible for its citrate competitive inhibition of ACL. Key interactions of **2a** with ACL are well defined in this binding orientation, and consist of pi-pi interactions with Phe-347, and H-bonding interactions of the 9-carbonyl and 8-OH functional groups with Asp-346 and Gly-664 (Fig. 3b). The 2-chloro, its adjacent 3-OH

Table 1

The SAR of emodin derivatives in inhibition of ACL enzymatic activity.

| Entry | Code | R ¹ | R ² | IC ₅₀ (μM) |
|-------|-------------------|------------------------------|----------------|------------------------------------|
| 1 | 1a | H | H | 0% ^a |
| 2 | 1b | Cl | H | 12.6 |
| 3 | 1c | H | Cl | 9.6 |
| 4 | 1d | Br | Br | 2.9 |
| 5 | 1e | I | H | 7.5 |
| 6 | 1f | Phenyl | H | 8% ^a |
| 7 | 1g | 3-Methylphenyl | H | 30.0 |
| 8 | 1h | 4-Methylphenyl | H | 0% ^a |
| 9 | 1i | 3-Methoxyphenyl | H | 21.2 |
| 10 | 1j | 4-Methoxyphenyl | H | 18.8 |
| 11 | 1k | 3,5-Dimethoxyphenyl | H | 0% ^a |
| 12 | 1l | 3-Pyridyl | H | 21.1 |
| 13 | 1m | 4-Pyridyl | H | 0% ^a |
| 14 | 1n | 3-Pyridyl | 3-pyridyl | 23.5 |
| 15 | 1o | 1-Methyl-4-pyrazolyl | H | 13.3 |
| 16 | 1p | 4-Morpholinylmethyl | H | 10% ^a |
| 17 | 1q | 1-Piperidinylmethyl | H | 6% ^a |
| 18 | 1r | N-Methyl-N-phenylaminomethyl | H | 6% ^a |
| 19 | 2a | Cl | H | 0.283 ^b |
| 20 | 2b | H | H | 0% ^a |
| 21 | 2c | H | Cl | 3.8 |
| 22 | 3a | Phenyl | H | 25.8 |
| 23 | 3b | 5-(1,3-Benzoxazolyl) | H | 29.7 |
| 24 | BMS-303141 | | | 0.442 |

^a % inhibition at 10 μM .

^b as reported in Ref. [18], and measured by the maleate dehydrogenase catalyzed reduction of oxaloacetate.

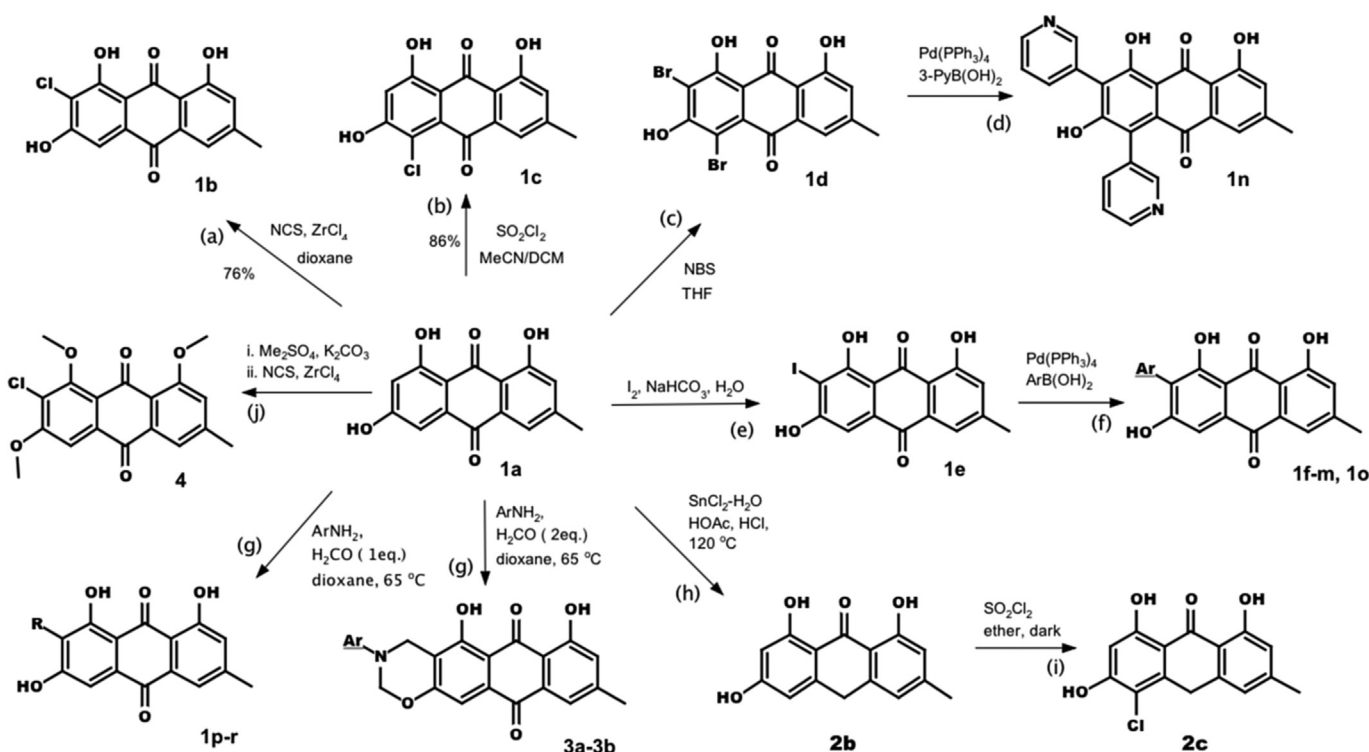


Fig. 1. Synthetic schemes for the preparation of emodin derivatives. Regioselective synthesis of the mono-chlorinated emodin **1b** (a) and **1c** (b). Synthesis of the bis-brominated emodin **1d** (c) and its Suzuki coupling for compound **1n** (d). Synthesis of the mono-iodinated emodin **1e** (e) and its Suzuki coupling for compounds **1f–m**, **1o** (f). Mannich reaction of emodin for the synthesis of **1p–r** and **3a–b** (g). Regioselective reduction of emodin for anthracenone **2b** (h) and its regioselective chlorination for **2c** (i). Synthesis of compound **4** (j). DCM: dichloromethane; MeCN: acetonitrile; NBS: N-bromosuccinimide; NCS: N-chlorosuccinimide; THF: tetrahydrofuran.

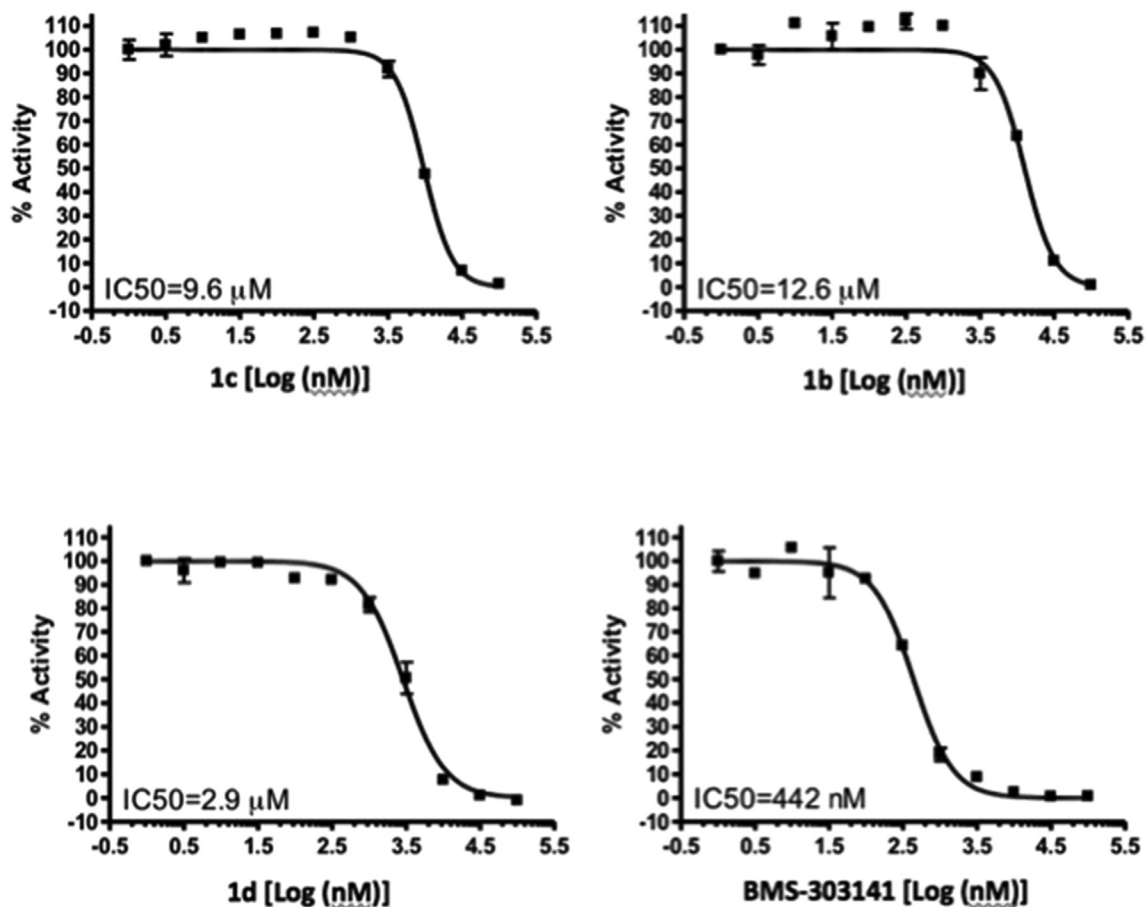


Fig. 2. Representative dose-response curves of ACL inhibition in the ADP-Glo enzymatic assay. Inhibitors were tested in duplicates at a dose range of 0.03–30 μM with 3.3-fold serial dilutions.

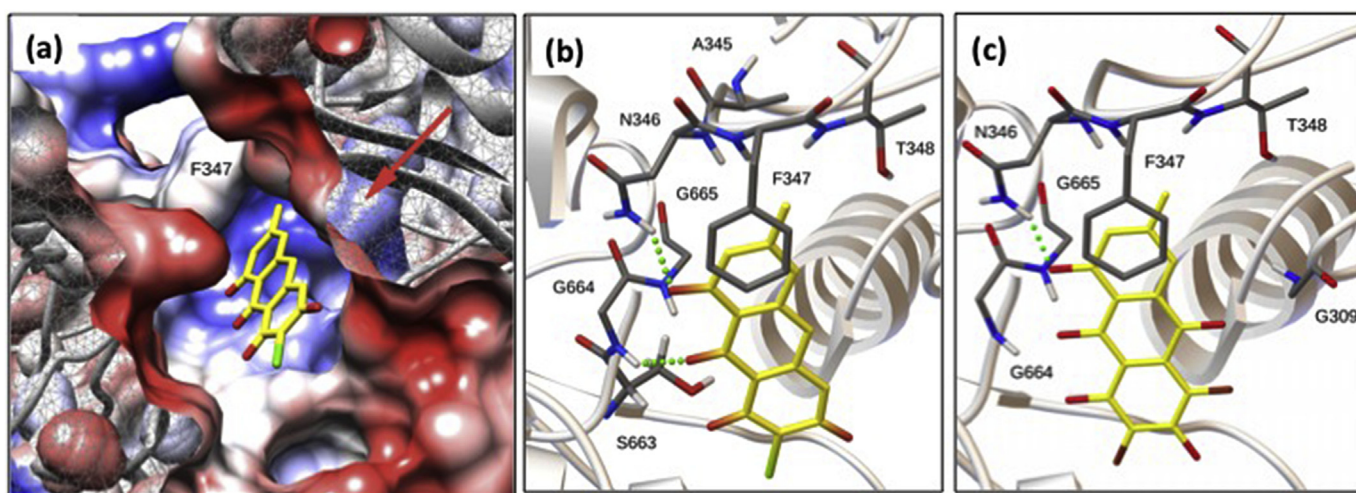


Fig. 3. (a) Space filling view of the lowest energy binding pose of **2a**. The anthraquinone was found to occupy space directly adjacent to the substrate binding domain (red arrow). Red and blue color indicates negatively or positively charged protein surface, respectively. (b) Key interactions found of **2a** with the ACL protein. The anthraquinone **2a** was found to participate in pi-pi interactions with Phe-347 and H-bonding interactions with Asp-346 and Gly-664 (indicated by green dash lines). (c) The lowest energy docking pose of **1d** indicates near identical interactions to that of **2a**. (For interpretation of the references to colour in this figure legend, the reader is referred to the web version of this article.)

functional groups, and the methylene linker at the 10-position of **2a** were not found to be involved in interactions with the ACL protein and a significant volume of space surrounding each functional group is unoccupied. This result corroborates our SAR results

demonstrating that variety of anthraquinone analogs with substituents at the 2–4 positions retain ACL inhibitory activity. Further, the lowest energy docking pose of **1d** (Fig. 3c) indicates that **1d** essentially forms the same interactions the as that for **2a**, with the

additional C-10 carbonyl group of **1d** extending to the solvents and lacking interactions with nearby amino acid residues.

2.4. Anti-proliferative activity

We tested the anticancer activity of selected ACL inhibitors in the A549 non-small cell lung cancer (NSCLC) cell line, which we had shown previously to be sensitive to ACL knockdown (KD) [11]. A549 cell harbors mutations in the KRAS oncogene and does not respond to molecular therapies that target the epithelial growth factor receptor (EGFR). We first treated A549 cells with 5 μM of the active ACL inhibitors **1b-d**, **1o**, and **2c** for 24 h and then measured by WST-1 reagent for cell proliferation. ACL KD was used as a positive control and to benchmark the activity of the inhibitors. At 5 μM concentration, our ACL inhibitors inhibited the A549 cell proliferation by 40–80% vs. 100% denoted to ACL KD (Fig. 4a). Furthermore, inhibitors **1d** and **1o** dose-dependently inhibited A549 cell proliferation (Fig. 4b–c). At 10 μM , **1d** was able to reach the same level of anticancer activity as achieved by ACL KD (100%), implying that at 10 μM **1d** full inhibits the cellular ACL activity in A549 cells, which correlates to its complete inhibition of ACL enzymatic activity in the enzymatic assay at similar dose levels (>99% inhibition at 3.3 and 10 μM).

It should be noted that emodin, which did not show any inhibition of ACL enzymatic activity at 10 μM (Table 1), is known to inhibit cancer cell proliferation via diverse mechanisms unrelated to ACL activity [36–38]. Thus, He et al. reported that treatment of the A549 lung cancer cell line with high concentrations (40 and 70 μM) of emodin led to significant inhibition of cell proliferation, presumably via down regulation of ERCC1 and Rad51 [37]. It is unclear whether the emodin derivatives tested in our studies retain some activities for those known targets and pathways. Therefore, we postulate that the emodin derivatives reported herein exert their anti-proliferative activity at least in part, but may not solely, via their inhibition of ACL. Future studies with more potent ACL inhibitors include selectivity measurements across a spectrum of reported pathways that are known to mediate the anticancer activity of emodin.

2.5. Reduction of cancer stemness

We had previously shown that shRNA KD of ACL in HMLE-Snail breast cancer cells and in A549 lung adenocarcinoma cells reduced cancer stemness [12]. We show here for the first time that small molecule ACL inhibitors are highly effective in altering cancer stemness. We applied the 3D spheroid assay [39,40] to evaluate the effect of the ACL inhibitor **1d** in modulating cancer stem cells. The FAK kinase inhibitor VS-6063 [41], which is known to target cancer

stem cells and currently under clinical investigations, and the ACL inhibitor BMS-303141 were included as positive controls. In this assay, effective agents for cancer stemness are expected to not only reduce the spheroid size (area size) but also induce apoptotic cells as detected by Sytox green. The intensity of Sytox Green correlated to the level of cellular damages, which was calculated as Intensity Density (IntDen). IntDen/Area was used as a readout index for an inhibitor's effectiveness in modulating cancer cell stemness. In both the A549 lung cancer cell line and the E-snail breast cell line, **1d** dose-dependently reduced the spheroid size and caused dramatic apoptosis in spheroid, indicating its strong inhibitory function for cancer stemness (Fig. 5A, B). Similarly but with less efficiency in the E-snail breast cancer cell line, the ACL inhibitor BMS-303141 also potently inhibited stemness in the cell based 3D assay.

3. Conclusions

In summary, we identified a new series of ACL inhibitors based on the chemical scaffold of the natural product emodin. SAR and docking analyses indicate that the two OH groups adjacent to the 9-carbonyl group may be critical for on-target activity. In addition, the auto docking studies indicated the formation of key interactions with N346 and G664 in an allosteric site adjacent to the citrate binding domain. Chemical modifications of the 2–5 positions of emodin lead to ACL inhibitors with IC_{50} ranging from 30 to 3 μM . Halogens at the 2- and 4-position of emodin increased activity most significantly, while aryl substituents at the 2-position of emodin resulted in moderately active ACL inhibitors. Lead compounds dose-dependently inhibited the proliferation of the A549 lung cancer cells, with the best compounds reaching to similar levels of activity to that of ACL KD. Further, we demonstrated for the first time that ACL inhibitors significantly reduced cancer stemness in the 3D spheroid assay. Our data provide further support to the approach of targeting ACL for treating cancers and will guide the future lead optimization studies.

4. Experimental section

4.1. Chemistry

4.1.1. General

All reagents and solvents were purchased from commercially available sources and used without further purification. All reactions were carried out according to the indicated procedures and conditions. Reactions were monitored by LC/MS analysis and/or thin-layer chromatography (TLC) on silica-coated glass or aluminum plates (EMD silica gel 60 F254) with the indicated eluent. The compounds were visualized by UV light (254 nm). LC/MS

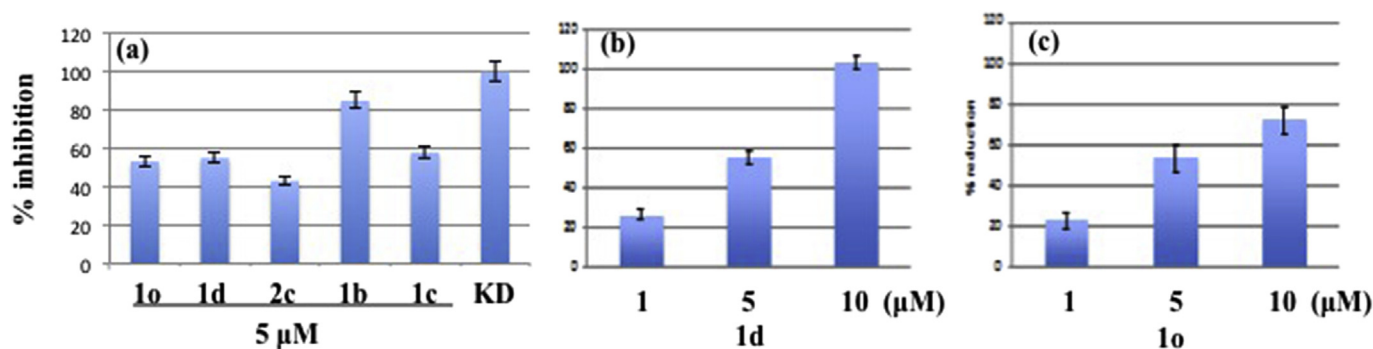


Fig. 4. Inhibition of A549 cancer cell proliferations. A549 cells were treated with (a) a single concentration (5 μM) or escalating doses (1, 5, 10 μM) of ACL inhibitors **1d** (b) and **1o** (c) for 24 h and then analyzed for proliferation. ACL knockdown (KD) by siRNA was included as positive control (not shown in (b) and (c)).

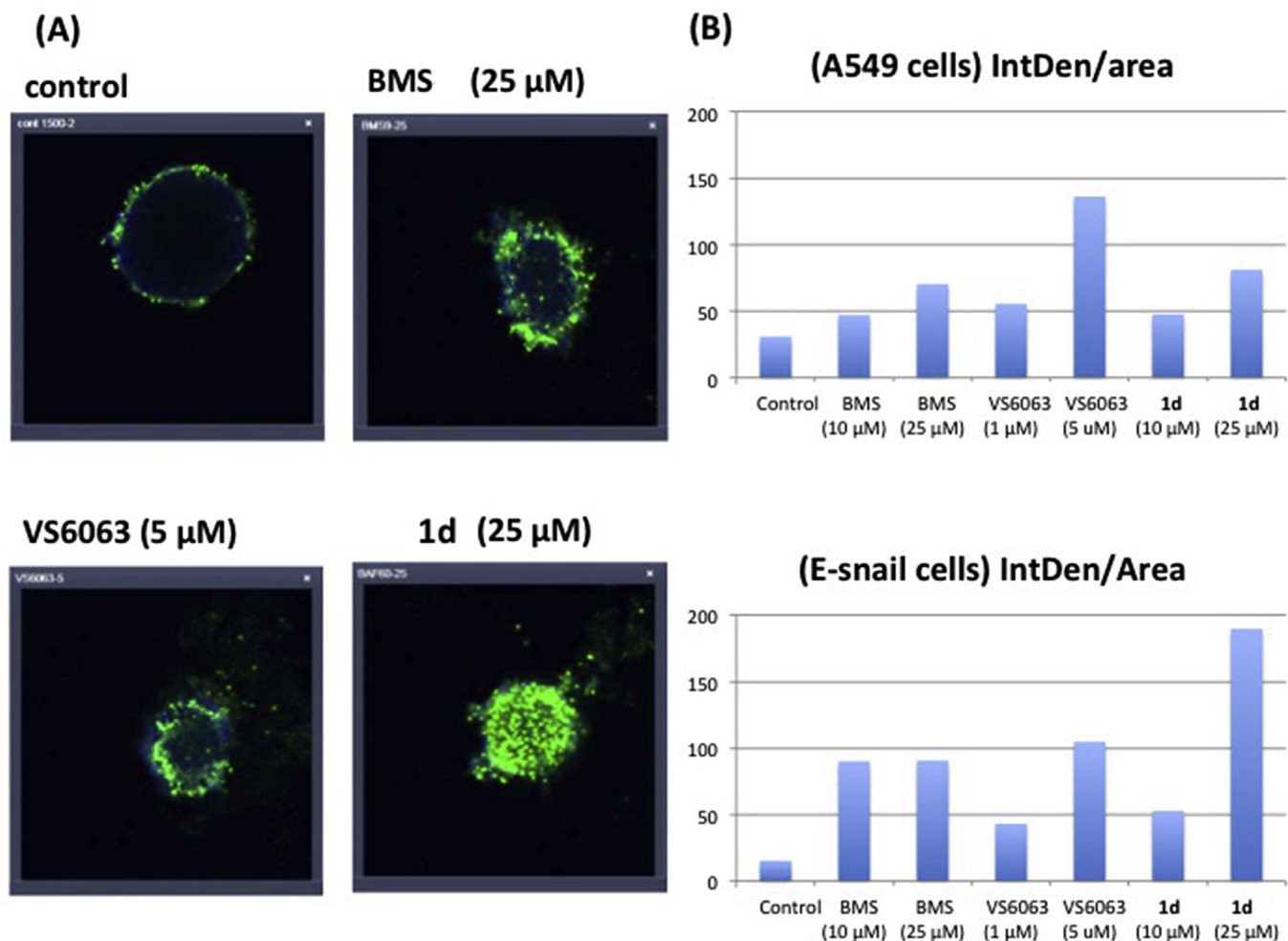


Fig. 5. Inhibition of cancer stemness in A549 lung and E-snail breast cancer cells. A549 and E-snail cells under the 3D culture condition were treated with the ACL inhibitors **1d** and BMS-303141, or the FAK inhibitor VS6063. Cells were analyzed for spheroid size and intensity density (IntDen). Representative confocal microscopic images of E-snail cells (A) and evaluation score (IntDen/Area) (B). Spheroid size (Area) was scaled down by inhibitors, which was calculated as an inner area of spheroid borders (blue). Cellular damages detected as an intensity of Sytox Green, which was calculated as Intensity Density (IntDen). (For interpretation of the references to colour in this figure legend, the reader is referred to the web version of this article.)

analysis was performed on an Agilent 1200 HPLC/UV (220 nm and/or 254 nm wavelength) system coupled with a mass spectroscopic (Applied Biosystems, MDS SCIEX, Q TRAP LC/MS/MS) detector. Compounds for analysis were dissolved in 100% DMSO and separated on C18 cartridge (particle size 2.6 μm , dimensions: 100 mm \times 2.1 mm, 0.3 mL/min flow rate, 1 mL injection volume) using acetonitrile/water mobile phase with 0.1% formic acid as a modifier. The gradient started at 20% acetonitrile, held for 2 min, and linearly increased to 97% acetonitrile over 10 min, with 3 min hold at 97% acetonitrile and subsequent re-equilibration to the original conditions in a total of 17 min. All compounds reported were obtained in a purity as >95% at 254 nm wavelength. Nuclear magnetic resonance (^1H NMR) spectra were recorded on a Varian Mercury plus NMR spectrometer operating at 400.13 MHz frequencies for ^1H , using a 5 mm ASW PFG probe capable of detecting ^1H , ^{13}C , ^{31}P , and ^{15}N nuclei. The proton chemical shifts (ppm) were referenced to the tetramethylsilane internal standard (0 ppm). NMR data are reported with these descriptions: s, singlet; d, doublet; t, triplet; q, quartet; m, multiplet; br, broad peak.

Emodin derivatives **1d**, **1e**, **1p-s**, and **3a-b** were synthesized by following reported procedures. Analytical data agreed with the assigned structures and reported values.

4.1.2. 2-Chloro-1,3,8-trihydroxy-6-methyl-anthracene-9,10-dione (**1b**)

A mix of Emodin (34 mg, 0.12 mmol) and ZrCl_4 (4.0 mg, 0.017 mmol, 0.14 eq) in dioxane (2.5 mL) was purged with argon for 30 min, heated to 70 $^\circ\text{C}$ over 40 min. To the resulting suspension was added a solution of NCS (22 mg, 0.16 mmol, 1.3 eq) in dioxane (0.5 mL) dropwise over 5 min at 70 $^\circ\text{C}$. The resulting reaction mix was stirred at 70 $^\circ\text{C}$ for 4 h, cooled to r.t. purified by silica gel chromatography to give the product as a yellow solid (29 mg, 76% yield). ^1H NMR agrees with literature report [21]. ^1H NMR (400 MHz, $\text{DMSO}-d_6$): δ 12.74 (s, 1H), 12.21 (s, br, 1H), 11.81 (s, 1H), 7.50 (s, 1H), 7.31 (s, 1H), 7.18 (d, $J = 0.8$ Hz, 1H), 2.41 (s, 3H).

4.1.3. 2-Chloro-1,3,8-trimethoxy-6-methyl-anthracene-9,10-dione (**4**)

The title compound was obtained analogously to **1b** by treating 1,3,8-trimethoxy-6-methyl-anthracene-9,10-dione with ZrCl_4 in dioxane. The ^1H NMR corresponds to the literature report.

^1H NMR (400 MHz, $\text{DMSO}-d_6$): δ 7.34 (s, 1H), 7.29 (s, 1H), 7.10 (s, 1H), 4.01 (s, 3H), 3.94 (s, 3H), 3.86 (s, 3H), 2.41 (s, 3H). MS (ESI+): m/z calc. for $[\text{C}_{18}\text{H}_{15}\text{ClO}_5]$ 346.06. Found: 347.3 $[\text{M}+\text{H}]^+$

4.1.4. 1-Chloro-2,4,5-trihydroxy-7-methyl-anthracene-9,10-dione (**1c**)

To a suspension of Emodin (132 mg, 0.5 mmol) in $\text{CHCl}_3/\text{MeCN}$ (5:1, 24 mL) was added a solution of SO_2Cl_2 in DCM (1.0 M, 2.5 mL, 5.0 eq) in one portion at room temperature. The resulting reaction mix was stirred at room temperature under nitrogen for 2 days, diluted with hexanes (50 mL), filter to collect the crude product as a yellow solid (128 mg, 86% yield). NMR agreed with literature report [20]. ^1H NMR (400 MHz, acetone- d_6): δ 12.83 (s, 1H), 11.87 (s, 1H), 10.39 (s, br, 1H), 7.57 (s, 1H), 7.17 (s, 1H), 6.86 (s, 1H), 2.49 (s, 3H). MS (ESI+): m/z calc. for $[\text{C}_{15}\text{H}_9\text{ClO}_5]$ 304.01. Found: 305.5 $[\text{M}+\text{H}]^+$

4.1.5. 1,3,8-Trihydroxy-2,4-dibromo-6-methyl-anthraquinone (**1d**)

To a stirred suspension of emodin (1.08 g, 4.0 mmol) in solvent of THF (100 mL) was added NBS (Bromosuccinimide 1.7 g, 9.6 mmol) at room temperature. After completion (LCMS) the reaction mixture was concentrated in vacuum. The crude product precipitated was filtered and further purified by flash column chromatography (silica gel; Hexanes: $\text{CH}_2\text{Cl}_2 = 3:1$ –100% CH_2Cl_2) to yield compound **2d** as a red solid. NMR agreed with literature report [25]. ^1H NMR (400 MHz, DMSO- d_6) δ 13.69 (s, 1H), 11.62 (s, 1H), 7.43 (s, 1H), 7.11 (s, 1H), 2.40 (s, 3H).

4.1.6. General procedure for the synthesis of 2-aryl emodins 1f–1m, **1o**

1,3,8-Trihydroxy-2-iodo-6-methyl-anthracene-9,10-dione (**1e**) (79.2 mg, 0.2 mmol) was dissolved in toluene (2 mL), ethanol (2 mL) and water (0.5 mL). Palladium tetrakis triphenylphosphine (46.2 mg, 0.04 mmol) was added. Aryl boronic acid (0.8 mmol) and saturated NaHCO_3 (0.5 mL) was added. The reaction mixture was degassed with argon for 10 min. The reaction mixture was heated to 80 °C for 12 h or until complete (indicated by TLC). After cooling to room temperature Ethyl acetate and water was added (10/10 mL). The organic phase was separated and dried over Na_2SO_4 . After filtration the solvent was removed *i. vac.* The crude residue was purified by prep. HPLC. Final purity was determined by LCMS. All reported compounds were obtained in purities of 95% and above.

4.1.7. 1,3,8-Trihydroxy-6-methyl-2-phenyl-9,10-dihydroanthracene-9,10-dione (**1f**)

^1H NMR (400 MHz, DMSO- d_6): δ 12.56 (s, 1H), 11.95 (s, 1H), 11.33 (s, 1H), 7.54 (d, $J = 1.6$ Hz, 1H), 7.34–7.42 (m, 6H), 7.19 (s, 1H), 2.42 (s, 3H). MS (ESI+): m/z calc. for $[\text{C}_{21}\text{H}_{14}\text{O}_5]$ 346.08. Found: 347.5 $[\text{M}+\text{H}]^+$.

4.1.8. 1,3,8-Trihydroxy-6-methyl-2-(3-methylphenyl)-9,10-dihydroanthracene-9,10-dione (**1g**)

^1H NMR (400 MHz, DMSO- d_6): δ 12.59 (s, 1H), 12.03 (s, 1H), 11.32 (s, 1H), 7.58 (s, 1H), 7.42 (s, 1H), 7.34 (t, $J = 7.2$ Hz, 1H), 7.23 (s, 1H), 7.16–7.19 (m, 3H), 2.47 (s, 3H), 2.35 (s, 3H). MS (ESI+): m/z calc. for $[\text{C}_{22}\text{H}_{16}\text{O}_5]$ 360.37 Found 361.7 $[\text{M}+\text{H}]^+$.

4.1.9. 1,3,8-Trihydroxy-6-methyl-2-(4-methylphenyl)-9,10-dihydroanthracene-9,10-dione (**1h**)

^1H NMR (400 MHz, DMSO- d_6): δ 12.55 (s, 1H), 11.96 (s, 1H), 11.28 (s, 1H), 7.53 (d, $J = 1.6$ Hz, 1H), 7.37 (s, 1H), 7.19–7.26 (m, 5H), 2.42 (s, 3H), 2.34 (s, 3H). MS (ESI+): m/z calc. for $[\text{C}_{22}\text{H}_{16}\text{O}_5]$ 360.37 Found 361.3 $[\text{M}+\text{H}]^+$.

4.1.10. 1,3,8-Trihydroxy-2-(3-methoxyphenyl)-6-methyl-9,10-dihydroanthracene-9,10-dione (**1i**)

^1H NMR (400 MHz, DMSO- d_6): δ 12.55 (s, 1H), 11.96 (s, 1H), 11.32 (s, 1H), 7.538 (d, $J = 1.6$ Hz, 1H), 7.35 (d, $J = 15.6$ Hz, 2H), 7.19 (s, 1H), 6.89–6.93 (m, 3H), 3.75 (s, 3H), 2.47–2.49 (m, 3H). MS (ESI+): m/z calc. for $[\text{C}_{22}\text{H}_{16}\text{O}_6]$ 376.36. Found 377.4 $[\text{M}+\text{H}]^+$.

4.1.11. 1,6,8-Trihydroxy-7-(4-methoxyphenyl)-3-methyl-2,3,9,10-tetrahydroanthracene-9,10-dione (**1j**)

^1H NMR (400 MHz, DMSO- d_6): δ 12.54 (s, 1H), 11.91 (s, 1H), 11.22 (s, 1H), 7.48 (s, 1H), 7.32 (s, 1H), 7.25–7.27 (dd, $J = 8.4$ Hz, 2.0 Hz, 2H), 7.14–7.16 (m, 2H), 6.93 (d, $J = 8.4$ Hz, 2H), 3.74 (s, 3H), 2.37 (s, 3H). MS (ESI+): m/z calc. for $[\text{C}_{22}\text{H}_{18}\text{O}_6]$ 376.1 Found 377.1 $[\text{M}+\text{H}]^+$.

4.1.12. 2-(3,5-Dimethoxyphenyl)-1,3,8-trihydroxy-6-methyl-9,10-dihydroanthracene-9,10-dione (**1k**)

^1H NMR (400 MHz, acetone- d_6): δ 12.64 (s, 1H), 12.09 (s, 1H), 7.62 (s, 1H), 7.49 (s, 1H), 7.18 (d, $J = 0.8$ Hz, 1H), 6.60 (d, $J = 2.4$ Hz, 2H), 6.52 (t, $J = 2.4$ Hz, 1H), 3.84 (s, 6H), 2.49 (s, 3H). MS (ESI+): m/z calc. for $[\text{C}_{23}\text{H}_{18}\text{O}_7]$ 406.39 Found 407.6 $[\text{M}+\text{H}]^+$.

4.1.13. 1,3,8-Trihydroxy-6-methyl-2-(pyridin-3-yl)-9,10-dihydroanthracene-9,10-dione (**1l**)

^1H NMR (400 MHz, DMSO- d_6): δ 12.59 (s, 1H), 11.84 (s, 1H), 11.59 (br s, 1H), 8.68 (br s, 1H), 8.53 (br s, 1H), 7.91 (br s, 1H), 7.68 (br s, 1H), 7.25 (s, 1H), 7.16 (s, 1H), 6.79 (s, 1H), 2.34 (s, 3H). MS (ESI+): m/z calc. for $[\text{C}_{20}\text{H}_{13}\text{NO}_5]$ 347.08 Found 348 $[\text{M}+\text{H}]^+$.

4.1.14. 1,3,8-Trihydroxy-6-methyl-2-(4-pyridyl)anthracene-9,10-dione (**1m**)

^1H NMR (400 MHz, DMSO- d_6): δ 12.69 (s, 1H), 11.92 (s, 1H), 8.70 (d, $J = 4.4$ Hz, 2H), 7.52–7.57 (m, 3H), 7.40 (s, 1H), 7.23 (s, 1H), 2.45 (s, 3H). MS (ESI+): m/z calc. for $[\text{C}_{20}\text{H}_{13}\text{NO}_5]$ 347.33 Found: 348.5 $[\text{M}+\text{H}]^+$.

4.1.15. 1,3,8-Trihydroxy-6-methyl-2-(1-methylpyrazol-4-yl)anthracene-9,10-dione (**1o**)

^1H NMR (400 MHz, DMSO- d_6): δ 13.24 (s, 1H), 11.95 (s, 1H), 11.71 (s, 1H), 8.34 (s, 1H), 8.15 (s, 1H), 7.52 (s, 1H), 7.38 (s, 1H), 7.19 (s, 1H), 3.90 (s, 1H), 2.47 (s, 3H). MS (ESI+): m/z calc. for $[\text{C}_{19}\text{H}_{14}\text{N}_2\text{O}_5]$ 350.32, Found 351.1 $[\text{M}+\text{H}]^+$.

4.1.16. 2,4,5-Trihydroxy-7-methyl-1,3-bis(pyridin-3-yl)-9,10-dihydroanthracene-9,10-dione (**1n**)

1,3-dibromo-2,4,5-trihydroxy-7-methyl-anthracene-9,10-dione **1d** (85.6 mg, 0.2 mmol) was dissolved in toluene (2 mL), ethanol (2 mL) and water (0.5 mL). Palladium tetrakis triphenylphosphine (46.2 mg, 0.04 mmol) was added. 3-Pyridyl boronic acid (123 mg, 1 mmol) and saturated NaHCO_3 (0.5 mL) was added. The reaction mixture was degassed with argon for 10 min. The reaction mixture was heated to 80 °C for 5 h. After cooling to room temperature Ethyl acetate and water was added (10/10 mL). The organic phase was separated and dried over Na_2SO_4 . After filtration the solvent was removed *i. vac.* The crude residue was purified by prep. HPLC. ^1H NMR (400 MHz, acetone- d_6): δ 12.31 (s, 1H), 11.91 (s, 1H), 8.75 (s, br, 1H), 8.70 (d, $J = 4.4$ Hz, 1H), 8.63 (d, $J = 6$ Hz, 1H), 8.61 (s, br, 1H), 7.68–7.65 (dd, $J = 8.4$ Hz, 5.2 Hz, 1H), 7.59–7.56 (dd, $J = 8.4$ Hz, 5.2 Hz, 1H), 7.34 (s, 1H), 7.15 (s, br, 1H), 2.44 (s, 3H). MS (ESI+): m/z calc. for $[\text{C}_{25}\text{H}_{16}\text{N}_2\text{O}_5]$ 424.4 Found 425.5 $[\text{M}+\text{H}]^+$.

4.1.17. 4-Chloro-1,3,8-trihydroxy-6-methyl-9,10-dihydroanthracen-9-one (**2c**)

1,3,8-trihydroxy-6-methyl-10H-anthracen-9-one (64 mg, 0.25 mmol) was dissolved in diethyl ether at room temperature. SO_2Cl_2 (1 M, 1.25 mL, 1.125 mmol) was added to the solution. The reaction was stirred at room temperature under exclusion of light for 25 h. The product was isolated by filtration and stored at –20 °C in the dark. ^1H NMR (400 MHz, acetone- d_6): δ 12.54 (s, 1H), 12.07 (s, 1H), 11.67 (s, 1H), 6.92 (s, 1H), 6.71 (s, 1H), 6.48 (s, 1H), 4.27 (s, 2H), 2.33 (s, 3H). ^{13}C -HSQC (400 MHz, DMSO- d_6): δ 120.4 (C5), 115.6 (C7), 102.2 (C2), 31.5 (C10), 21.1 (CH3). ^{13}C -HMBC (400 MHz, DMSO- d_6): δ C5-correlation with CH₃ and C10, C7 correlation with CH₃, C2

no correlation with C10. MS (ESI+): m/z calc. for $[C_{15}H_{11}ClO_4]$ 290.03. Found: $[M+H]^+$

4.2. Docking study

The two-dimensional structure and ionization state of the natural product anthracenone **2a** were drawn in two dimensions using MarvinDraw (Marvin 6.2.2, 2014, ChemAxon: <http://www.chemaxon.com>). **2a** was converted into a low energy three-dimensional structure using Openbabel (v2.3.2) [42]. The ACL crystal structure (PDB: 3MWD) and small molecule **2a** were prepared for docking using Autodocktools (v1.5.6) [43]. Autodocking was performed using Autodock Vina (v1.1.2) and following the standard published docking protocol [44]. The low energy binding pose of **2a** relative to ACL was visualized using a combination of Autodocktools (v1.5.6) and USCF chimera (v1.11) [43], [45].

4.3. Enzymatic assay

The assay was performed using ADP-Glo luminescence assay reagents. It measures ACLY activity by quantification of the amount of ADP generated by the enzymatic reaction. The luminescent signal from the assay is correlated with the amount of ADP generated and is proportionally correlated with the amount of ACLY activity. The compounds were diluted in 10% DMSO and 2.5 μ l of the dilution was added to a 25 μ l reaction so that the final concentration of DMSO is 1% in all of reactions. All of the enzymatic reactions were conducted at 30 °C for 60 min. The 25 μ l reaction mixture contains 40 mM Tris, pH 8.0, 10 mM $MgCl_2$, 5 mM DTT, ATP, CoA, and Sodium Citrate and ACLY. After the enzymatic reaction, 25 μ l of ADP-Glo reagent was added to each reaction and incubate the plate for 45 min at room temperature. After then, 50 μ l of Kinase Detection reagent was added and incubated for 60 min at room temperature. The luminescence signal was measured using a Bio-Tek Synergy 2 microplate reader.

4.4. Proliferation assay (WST-1)

A549 cells were seeded in a 96-well plate at a density of 5×10^4 cells/well in 100 μ l of Ham's F-12 medium supplemented with 10% FBS, with or without compounds to be tested, and cultured for 24, 48, 72 h in a CO_2 incubator at 37 °C in 5% CO_2 . At each time point of measurement, WST-1 reagent (Roche Diagnostics, 10 μ l) were added to each well, and after 1 h incubation in a CO_2 incubator, the absorbance of each well was measured using a microplate reader (Beckman Coulter DTX880 multimode detector) at a wavelength of 450 nm.

4.5. 3D spheroid assay and evaluation

4.5.1. Spheroid generation

50 μ l of a heated 1.5% w/v agarose (Sigma A9539; in DMEM without fetal bovine serum (FBS)) solution was dispensed into sterile 96-well clear bottom imaging plates. For tumor spheroid seeding, suspended cells in regular medium (100 μ l) were added into agarose-coated well. Cell number for seeding was optimized for each cell lines to obtain spheroids with an approximate diameter of 400 μ m on day 5: 2000 cells per well (c/w) for A549 lung adenocarcinoma cells and HMLE-Snail breast cancer cells. The plates were incubated under standard cell culture conditions at 37 °C and 5% CO_2 in humidified incubators for 2 days to allow formation of reproducible spheroids of defined size and morphology, followed by adding each reagent (in 100 μ l culture medium) for additional 3 days.

Prior to imaging, spheroids were stained for 24 h by adding 20 μ l

of the mixed staining solution; Hoechst 33342 (1 mg/mL, Life Technologies) as counterstain for all nuclei and Sytox Green, as stain for dead cells (2 mM, Life Technologies) at a final dilution of 1:10,000 each.

4.5.2. Image acquisition and analysis

3D images were acquired by confocal microscopy (Zeiss LSM 510 Meta), focusing on the spheroid center. Each image was analyzed by ImageJ, by splitting into Hoechst (blue) image and Sytox Green image. Spheroid size (Area) was scaled down by effective reagents, which was calculated as an inner area of spheroid borders (Hoechst channel). Cellular damages detected as an intensity of Sytox Green, which was calculated as Intensity Density (IntDen). IntDen/Area was used as a readout index for inhibitors effectiveness.

Competing interests

The authors declared no competing interests.

Author's contributions

SKK and SB synthesized the compounds. FEJ conducted the modeling study. JH, MO, CK, and SE carried out biological assays. SKK, FEJ, JH, VS, and LS drafted the manuscript. VS and LS conceived and directed the studies. All authors read and approved the manuscript.

Acknowledgement

This research is partially supported by a seed fund for the Center for Drug Discovery and Translational Research (LS) and a research grant by Fujifilm (VPS and LS). The Sponsors played no roles in study design, the collection, analysis and interpretation of data, the writing of the report, and the decision to submit the article for publication. We thank Charles Sheehan of the NMR Core of Harvard Medical School for his critical advice on ^{13}C -HMBC/ ^{13}C -HSQC experiments and structural determinations of compound **2c**, and BPS Bioscience for technical support in the ADP Glo enzymatic assay.

Appendix A. Supplementary data

Supplementary data related to this article can be found at <http://dx.doi.org/10.1016/j.ejmech.2016.12.018>.

References

- [1] L. Galluzzi, O. Kepp, M.G. Vander Heiden, G. Kroemer, Metabolic targets for cancer therapy, *Nat. Rev. Drug Disc.* 12 (2013) 829–846.
- [2] M. Jang, S.S. Kim, J. Lee, Cancer cell metabolism: implications for therapeutic targets, *Exp. Mol. Med.* 45 (2013) e45.
- [3] R.A. Cairns, I.S. Harris, T.W. Mak, Regulation of cancer cell metabolism, *Nat. Rev. Cancer* 11 (2011) 85–95.
- [4] G. Hatzivassiliou, F. Zhao, D.E. Bauer, C. Andreadis, A.N. Shaw, D. Dhanak, S.R. Hingorani, D.A. Tuveson, C.B. Thompson, ATP citrate lyase inhibition can suppress tumor cell growth, *Cancer Cell* 8 (2005) 311–321.
- [5] M. Board, E. Newsholme, Hydroxycitrate causes altered pyruvate metabolism by tumorigenic cells, *Biochem. Mol. Biol. Int.* 40 (1996) 1047–1056.
- [6] R.J. DeBerardinis, J.J. Lum, G. Hatzivassiliou, C.B. Thompson, The biology of cancer: metabolic reprogramming fuels cell growth and proliferation, *Cell Metab.* 7 (2008) 11–20.
- [7] P.F. McAndrew, Fat metabolism and cancer, *Surg. Clin. North. Am.* 66 (1986) 1003–1012.
- [8] J.V. Swinnen, K. Brusselmans, G. Verhoeven, Increased lipogenesis in cancer cells: new players, novel targets, *Curr. Opin. Clin. Nutr. Metab. Care* 9 (2006) 358–365.
- [9] Y. Zhou, L.R. Bollu, F. Tozzi, X. Ye, R. Bhattacharya, G. Gao, E. Dupre, L. Xia, J. Lu, F. Fan, S. Bellister, L.M. Ellis, Z. Weihua, ATP citrate lyase mediates resistance of colorectal cancer cells to SN38, *Mol. Cancer Ther.* 12 (2013) 2782–2791.
- [10] K.E. Wellen, G. Hatzivassiliou, U.M. Sachdeva, T.V. Bui, J.R. Cross, C.B. Thompson, ATP-citrate lyase links cellular metabolism to histone

- acetylation, *Science* 324 (2009) 1076–1080.
- [11] J. Hanai, N. Doro, A.T. Sasaki, S. Kobayashi, L.C. Cantley, P. Seth, V.P. Sukhatme, Inhibition of lung cancer growth: ATP citrate lyase knockdown and statin treatment leads to dual blockade of mitogen-activated protein kinase (MAPK) and phosphatidylinositol-3-kinase (PI3K)/AKT pathways, *J. Cell. Physiol.* 227 (2012) 1709–1720.
- [12] J.I. Hanai, N. Doro, P. Seth, V.P. Sukhatme, ATP citrate lyase knockdown impacts cancer stem cells in vitro, *Cell Death Dis.* 4 (2013) e696.
- [13] A.D. Khwairakpam, M.S. Shyamananda, B.L. Sailo, S.R. Rathnakaram, G. Padmavathi, J. Kotoky, A.B. Kunnumakkara, ATP citrate lyase (ACLY): a promising target for cancer prevention and treatment, *Curr. Drug Targets.* 16 (2015) 156–163.
- [14] X.Y. Zu, Q.H. Zhang, J.H. Liu, R.X. Cao, J. Zhong, G.H. Yi, Z.H. Quan, G. Pizzorno, ATP citrate lyase inhibitors as novel cancer therapeutic agents, *Recent Pat. Anticancer Drug Disc.* 7 (2012) 154–167.
- [15] N. Zaidi, I. Royaux, J.V. Swinnen, K. Smans, ATP citrate lyase knockdown induces growth arrest and apoptosis through different cell- and environment-dependent mechanisms, *Mol. Cancer Ther.* 11 (2012) 1925–1935.
- [16] N. Zaidi, J.V. Swinnen, K. Smans, ATP-citrate lyase: a key player in cancer metabolism, *Cancer Res.* 72 (2012) 3709–3714.
- [17] A. Liu, H. Chen, W. Wei, S. Ye, W. Liao, J. Gong, Z. Jiang, L. Wang, S. Lin, Antiproliferative and antimetastatic effects of emodin on human pancreatic cancer, *Oncol. Rep.* 26 (2011) 81–89.
- [18] J.J. Oleynek, C.J. Barrow, M.P. Burns, D.M. Sedlock, D.J. Murphy, P.V. Kaplita, H.H. Sun, R. Cooper, A.M. Gillum, C.C. Chadwick, Anthrones, naturally occurring competitive inhibitors of adenosine-triphosphate-citrate lyase, *Drug Dev. Res.* 36 (1995) 35–42.
- [19] I. Yosioka, H. Yamauchi, K. Morimoto, I. Kitagawa, Two new chlorine containing anthraquinones from a lichen, *anaptychia obscurata* (nyl.), *Tetrahedron Lett.* 9 (1968) 1149–1152.
- [20] Q.H.Y. Chen, W. Huang, Emodin Derivative and its Application as Antibacterial Agents, 2012. CN 102775291.
- [21] M.V. Sargent, D.O.N. Smith, J.A. Elix, The minor anthraquinones of *Xanthoria parietina*(L.) Beltram, the chlorination of parietin, and the synthesis of fragilin and 7-chloroemodin ('AO-1'), *J. Chem. Soc. C. Org.* (1970) 307–311.
- [22] M.A. Elban, S.M. Hecht, Total synthesis of the topopyrones: a new class of topoisomerase I poisons, *J. Org. Chem.* 73 (2008) 785–793.
- [23] M. Koyama, K. Takahashi, T.C. Chou, Z. Darzynkiewicz, J. Kapuscinski, T.R. Kelly, K.A. Watanabe, Intercalating agents with covalent bond forming capability. A novel type of potential anticancer agents. 2. Derivatives of chrysophanol and emodin, *J. Med. Chem.* 32 (1989) 1594–1599.
- [24] S.B. Kalidhar, Structural elucidation in anthraquinones using ¹H NMR glycosylation and alkylation shifts, *Phytochem* 28 (1989) 3459–3463.
- [25] F. Duan, X. Li, S. Cai, G. Xin, Y. Wang, D. Du, S. He, B. Huang, X. Guo, H. Zhao, R. Zhang, L. Ma, Y. Liu, Q. Du, Z. Wei, Z. Xing, Y. Liang, X. Wu, C. Fan, C. Ji, D. Zeng, Q. Chen, Y. He, X. Liu, W. Huang, Haloemodin as novel antibacterial agent inhibiting DNA gyrase and bacterial topoisomerase I, *J. Med. Chem.* 57 (2014) 3707–3714.
- [26] J.-M. Lapierre, S. Eathiraj, D. Vensel, Y. Liu, C.O. Bull, S. Cornell-Kennon, S. Iimura, E.W. Kelleher, D.E. Kizer, S. Koerner, S. Makhija, A. Matsuda, M. Moussa, N. Namdev, R.E. Savage, J. Szwaya, E. Volckova, N. Westlund, H. Wu, B. Schwartz, Discovery of 3-(3-(4-(1-aminocyclobutyl)phenyl)-5-phenyl-3H-imidazo[4,5-b]pyridin-2-yl)pyridin-2-amine (ARQ 092): an orally bioavailable, selective, and potent allosteric AKT inhibitor, *J. Med. Chem.* 59 (2016) 6455–6469.
- [27] L.-M. Zhao, L.-M. Zhang, F.-Y. Ma, X.-S. Wang, H.-S. Jin, Catalyst-free Mannich reaction of hydroxyanthraquinone: facile access to emodin Mannich bases and anthraoxazines, *Tetrahedron Lett.* 54 (2013) 2802–2805.
- [28] J.L. Liang, H.C. Cha, S.H. Lee, J.-K. Son, H.W. Chang, J.-E. Eom, Y. Kwon, Y. Jahng, A facile synthesis of emodin derivatives, emodin carbaldehyde, citreorosein, and their 10-deoxygenated derivatives and their inhibitory activities on μ -calpain, *Arch. Pharm. Res.* 35 (2012) 447–454.
- [29] B. Shroot, C. Brown, Free radicals in skin exposed to dithranol and its derivatives, *Arzneimittelforschung* 36 (1986) 1253–1255.
- [30] J. Fuchs, L. Packer, Investigations of anthralin free radicals in model systems and in skin of hairless mice, *J. Invest. Dermatol.* 92 (1989) 677–682.
- [31] A.D. Gribble, R.E. Dolle, A. Shaw, D. McNair, R. Novelli, C.E. Novelli, B.P. Slingsby, V.P. Shah, D. Tew, B.A. Saxty, M. Allen, P.H. Groot, N. Pearce, J. Yates, ATP-citrate lyase as a target for hypolipidemic intervention. Design and synthesis of 2-substituted butanedioic acids as novel, potent inhibitors of the enzyme, *J. Med. Chem.* 39 (1996) 3569–3584.
- [32] F. Fan, H.J. Williams, J.G. Boyer, T.L. Graham, H. Zhao, R. Lehr, H. Qi, B. Schwartz, F.M. Raushel, T.D. Meek, On the catalytic mechanism of human ATP citrate lyase, *Biochemistry* 51 (2012) 5198–5211.
- [33] J.J. Li, H. Wang, J.A. Tino, J.A. Robl, T.F. Herpin, R.M. Lawrence, S. Biller, H. Jamil, R. Ponticello, L. Chen, C.H. Chu, N. Flynn, D. Cheng, R. Zhao, B. Chen, D. Schnur, M.T. Obermeier, V. Sasseville, R. Padmanabha, K. Pike, T. Harrity, 2-hydroxy-N-arylbenzenesulfonamides as ATP-citrate lyase inhibitors, *Bioorg. Med. Chem. Lett.* 17 (2007) 3208–3211.
- [34] Z. Ma, C.H. Chu, D. Cheng, A novel direct homogeneous assay for ATP citrate lyase, *J. Lipid Res* 50 (2009) 2131–2135.
- [35] T. Sun, K. Hayakawa, K.S. Bateman, M.E. Fraser, Identification of the citrate-binding site of human ATP-citrate lyase using X-ray crystallography, *J. Biol. Chem.* 285 (2010) 27418–27428.
- [36] H.Z. Lee, Effects and mechanisms of emodin on cell death in human lung squamous cell carcinoma, *Br. J. Pharmacol.* 134 (2001) 11–20.
- [37] L. He, J.J. Bi, Q. Guo, Y. Yu, X.F. Ye, Effects of emodin extracted from Chinese herbs on proliferation of non-small cell lung cancer and underlying mechanisms, *Asian Pac. J. Cancer Prev.* 13 (2012) 1505–1510.
- [38] G. Srinivas, S. Babykutty, P.P. Sathiadevan, P. Srinivas, Molecular mechanism of emodin action: transition from laxative ingredient to an antitumor agent, *Med. Res. Rev.* 27 (2007) 591–608.
- [39] C. Wenzel, B. Riefke, S. Grundemann, A. Krebs, S. Christian, F. Prinz, M. Osterland, S. Golfer, S. Rase, N. Ansari, M. Esner, M. Bickle, F. Pampaloni, C. Mattheyer, E.H. Stelzer, K. Parczyk, S. Prechtel, P. Steigemann, 3D high-content screening for the identification of compounds that target cells in dormant tumor spheroid regions, *Exp. Cell Res.* 323 (2014) 131–143.
- [40] J. Friedrich, C. Seidel, R. Ebner, L.A. Kunz-Schughart, Spheroid-based drug screen: considerations and practical approach, *Nat. Protoc.* 4 (2009) 309–324.
- [41] F.J. Sulzmaier, C. Jean, D.D. Schlaepfer, FAK in cancer: mechanistic findings and clinical applications, *Nat. Rev. Cancer* 14 (2014) 598–610.
- [42] N.M. O'Boyle, M. Banck, C.A. James, C. Morley, T. Vandermeersch, G.R. Hutchison, Open Babel: An open chemical toolbox, *J. Cheminform* 3 (2011) 33.
- [43] G.M. Morris, R. Huey, W. Lindstrom, M.F. Sanner, R.K. Belew, D.S. Goodsell, A.J. Olson, AutoDock4 and AutoDockTools4: Automated docking with selective receptor flexibility, *J. Comput. Chem.* 30 (2009) 2785–2791.
- [44] O. Trotter, A.J. Olson, AutoDock Vina: improving the speed and accuracy of docking with a new scoring function, efficient optimization, and multi-threading, *J. Comput. Chem.* 31 (2010) 455–461.
- [45] E.F. Pettersen, T.D. Goddard, C.C. Huang, G.S. Couch, D.M. Greenblatt, E.C. Meng, T.E. Ferrin, UCSF Chimera—a visualization system for exploratory research and analysis, *J. Comput. Chem.* 25 (2004) 1605–1612.